Corrosion and Stress Corrosion Resistance of Al Zn Alloy 7075 by Nano-Polymeric Coatings

Amal M. Abdel-Karim[1] · Ashraf M. El-Shamy[1] · Y. Reda[2]

Abstract

Al–Zn alloy 7075 has been broadly considered owing to its exceptional machinery possessions established by age hardening and extensive uses. For instance, the creation of stress corrosion cracking is an example of stress corrosion. Stress corrosion cracking is caused by a corrodent reacting with long-term, continuous tensile stress. Stress corrosion cracking is sometimes referred to as stress corrosion cracking or stress corrosion cracking. It is characterized by corrosion in the microscopic granular composition of a metal's surface, which leads to the production of a rusty surface on the metal's surface. Small cracks on the metallic surface are formed as a consequence of the application of stresses (applied or residual), which causes the boundaries to open and cracks to emerge. It is noticed from the values of corrosion potential and R_p increased, while the values of corrosion current density and corrosion rate are diminished by polyurethane PU coating more than polyamide PA and nitrocellulose NC, confirming that PU coverings afford an operative shield against deterioration of Al7075, suggesting the excessive possibility for application in industry. The morphology of Al alloy coated with polymer was characterized using SEM. The PU is recommended as a coating polymer for shielding the surface of Al.

Keywords Al alloy 7075 · Polyurethane · Polyamide · Nitrocellulose · Stress Corrosion Cracking

1 Introduction

Al is a popular metal used in industrial applications [1–3]. This is owing to several factors, including a massively strong argument for mass breaking, corrosion resistance, a low specific gravity 2.72, lightweight, and ease of fabrication. Al in its purest form is a brittle yet malleable metal. When stressed, Al deforms three times more than steel, and the casting procedure has not addressed this issue [4–8]. Al alloys, unlike steel and titanium, are extremely strong while retaining their ductility [9–11]. Stress annealing or cold working can significantly improve the strength of this and other Al alloys. Al alloys can be strengthened with several constituents [12–15]. Whereas in 7xxx series compounds, Zn is the predominant alloying component in amounts ranging from 1 to 8%, resulting in a high-strength, heat-treatable alloy when combined with a reduced proportion of Mg. Other elements, like Cu and Cr, can be used in tiny amounts in aircraft structures and portable devices. Because of its resistance to deterioration and fracture, alloy 7xxx has shown to be more successful in resisting stress corrosion and has been used more frequently at high temperatures [16–20]. Several corrosion protection methods, such as organic or inorganic antirust and metal coatings, are used to build defensive coatings that restrict the rate of corrosion and extend the life of these alloys. Among these helpful coatings are polymers, which have a high potential to protect metals against corrosion [21–23]. When using polymers, it is recommended that they have advantages such as the ability to form a strong physical barrier and that they be strengthened with an additional PU coating class, NC. Both PU and NC are based on epoxy PA to ensure good adherence between the substrate and the final coat [24–26]. The most important of these coatings, PU, uses a high-strength aliphatic coating with low VOC. As a result, PU coatings are recommended for regularly used coating systems used to protect steel buildings in very corrosive conditions other

✉ Ashraf M. El-Shamy
  elshamy10@yahoo.com; am.elshamy@nrc.sci.eg

1 Electrochemistry and Corrosion Laboratory, Physical Chemistry Department, National Research Centre, 33, El-Bohouth St. Dokki, P.O. 12622, Giza, Egypt

2 Chemical Engineering Department Higher Institute of Engineering and Technology Tanta, Canal High Institute of Engineering and Technology, Tanta, Egypt

than seawater [27, 28]. As a result, the purpose of this study was to assess different polymers and their effects on preventing stress corrosion in the Al–Zn 7075 alloy used in the aircraft frame construction [29].

2 Experimental

The alloy used is Al–Zn 7075 with a thickness of about 0.5 mm, with a submerged area of about 1 cm^2. PA, NC, NaCl, and PU were used as materials to investigate in this article. The alloy selected is subjected to an XRF analyzer Thermo Scientific Niton XL3T regulating the % of each metal. Chemical analysis of Al 7075; Zn 5.70, Mg 2.40, Cu 1.60, Mn 0.30, Si 0.40, Fe 0.50, Cr 0.20, Ti 0.20, Al 88.55 and 0.15% total as mentioned in Table 1.

The Al–Zn 7075 alloy samples were plotted by applying acetone as a degreaser to remove oil or imprint on the samples, to ensure proper bonding of the applied layer. The electrochemical experiments are carried out using a normal electrochemical cell used a computer-aided Autolab potentiostat/galvanostat device PGSTAT302N is a three-electrode cell at room temperature. The saturated calomel electrode was used as a reference electrode, and the counter electrode was fixed with platinum foil. Coated and uncoated work electrodes were used for the Al alloy samples. The working electrode area of about 1.0 cm^2 with and without a coat was exposed to 3.5% NaCl. The OCP was recorded for at least 30 min before each experiment. And the frequency range over AC from 0.1 to 105 Hz with a low-to-low sine wave of ± 10 mV as the excitation signal. Both polarization experiments were performed at a scanning speed of 1.0 mV at 1 and laboratory temperature within the potential range from -0.8 to 0.1 V. The surface topography of the coated Al in the normal and stress-corrosive condition is performed in saline media after 12 h immersion via a JEOL JAX-840A SEM electron microscope analyzer [30].

3 Results and Discussion

3.1 Open Circuit Potential Measurements

The gap in free corrosion potentials in 3.5% NaCl with time for uncoated and PA, NC, and/or PU-coated Al7075 is present in Fig. 1a. The stable OCP values in both the untreated and treated Al7075 were obtained after 30 min of immersion. For the coated sample a positive variation of the OCP
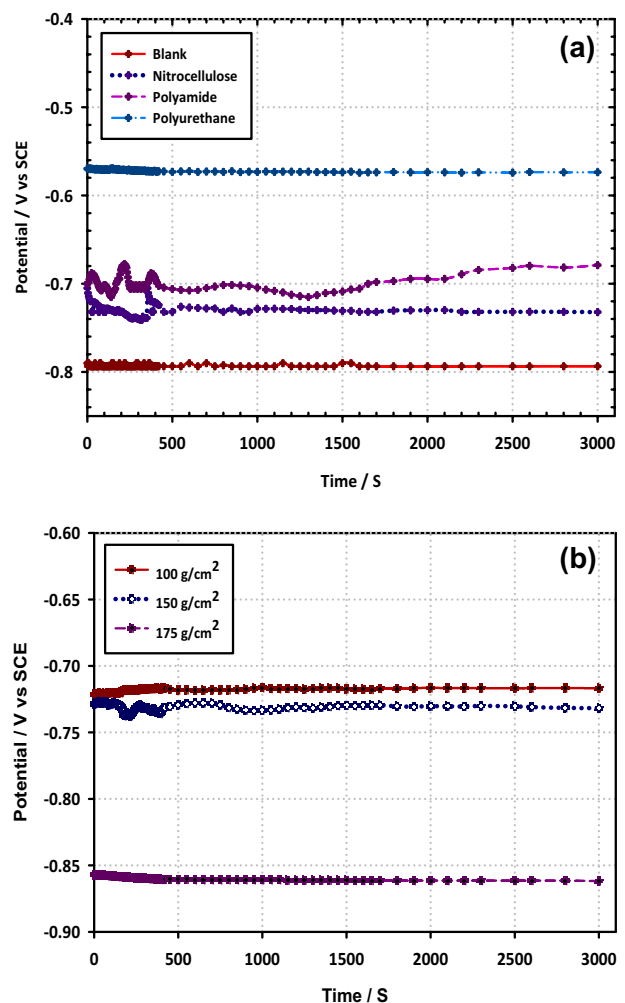

Fig. 1 The recorded OCP throughout immersion in 3.5% NaCl solution for **a** corrosion and **b** stress corrosion of uncoated Al 7075 alloy at the ambient temperature

was observed in respect of the untreated specimen in the corrosive medium. The steady OCP for uncoated and NC, PA, and/or PU-coated are -790 mV, -740, -680, and -577 mV, respectively. This conduct designates that; the coated PU is the highest positive potential shift. So it is the effective polymer for inhibition of the 7075- alloy relative to PA and NC. Under stress, it was observed that the possible potential of steady-state for the untreated alloy was shifted to more negative values. The OCP for 100,150 and 175 g m^{-2} are -720, -742 and -865 mV as seen in Fig. 1b.

Table 1 Elemental analysis of Al 7075 alloy	Element	Zn	Mg	Cu	Mn	Si	Fe	Cr	Ti	Al
	%	5.7	2.4	1.6	0.3	0.4	0.5	0.2	0.2	88.55

3.2 Measurements of Potentiodynamic Polarization PD

Figure 2a displays the measurements of PD curves of untreated and treated Al–Zn 7075 alloy in 3.5% NaCl at lab temperature, with a scanning rate of around 1 mV s^{-1} varying from − 0.8 to 0.1 mV from the OCP values. All curves tend to show the same general characteristics. The cathodic region shows a restrictive current density connected with the diffusion-controlled oxygen reduction reaction. Table 2 lists the parameters of PD such as i_{corr} current density, E_{corr} corrosion potential, R_p anodic β_a, and cathodic β_c Tafel slopes. The E_{corr} and i_{corr} principles were gotten by extrapolating the linear portion of both Tafel curves and the inhibition efficiencies were calculated [31]. The inhibition efficiencies for NC, PA, and PU are measured in the following order 65, 92, and 96%, respectively. The uncoated Al alloys Icorr was 1.19×10^{-5} A cm^{-2}. The I$_{corr}$ was moved to 8.47×10^{-6}, 2.06×10^{-6}, and 4.38×10^{-8} A cm^{-2} for NC, PA, and PU coating. Crosslink capability of PU results from containing two or more groups of isocyanates. The PU coating demonstrated the greatest anti-corrosion capabilities compared to PA and NC coating, as indicated by its highest and lowest values for R_p and I_{corr}, respectively. PA and NC matrix has low coating resistance and easy design of conductive. However, at a consistent time, filling the micropores of the polymeric matrix influence the barrier effect which gives the high protective features of the coating. Figure 2b shows uncoated Al alloy behavior under 100,150 and 175 gm cm^{-2} stresses. The stress corrosion potentials were − 0.983, − 1.16, and − 1.04 V, respectively. This stress 175 g m^{-2} was then loaded to the coated alloy as publicized in Fig. 2c. The potential for uncoated, NC, PA and, PU-coated samples were − 1.041, − 1.039, − 1.173, and − 1.12 V, respectively. The parameters of corrosion results are listed in Table 2. It is found that the current density shifted to less value 6.24×10^{-7} A cm^{-2} and the resistance increased for PU coating. It indicated that the most protective coating is PU because it forms a shield between the corrosive species and the metallic superficial [32–35].

3.3 Electrochemical Impedance Measurements (EIS)

Figure 3a demonstrates the semi-circular for uncoated sample indicates the corrosion process was regulated by the charge transfer resistance. However, in the attendance of polymeric paint, the increased semicircular is regarded as an indicator of the R_p between the metal and the external Helmholtz plane. The Nyquist plot of PU coating was nearly semicircle arcs. We found that the charge transfer resistances of the samples, as determined by the intersection of the low-frequency end of each semicircle arc with the real axis, were $3 \times 10^6 \ \Omega$ cm^2. However, the EIS semicircles rely
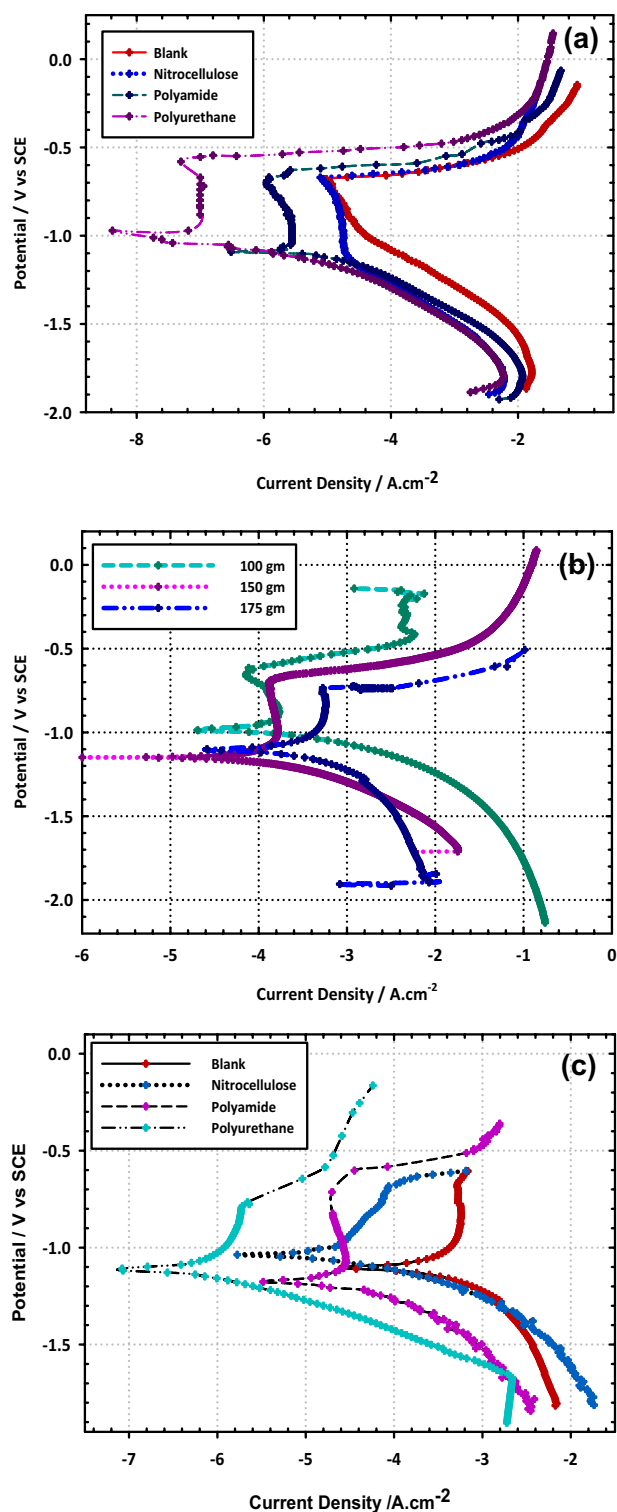

Fig. 2 The recorded potentiodynamic polarization curves of **a** corrosion, **b** stress corrosion of uncoated and **c** stress corrosion of 175 g cm^{-2} of uncoated and coated Al 7075 alloy in 3.5% NaCl, at ambient temperature and the scan rate of about 1 mV s^{-1}

Table 2 Electrochemical parameters and inhibition efficiency of corrosion and stress corrosion for coated and uncoated Al7075 alloy in 3.5% NaCl

Materials	E, (V) vs. SCE	b_a (V dec^{-1})	b_c (V dec^{-1})	I_{corr} (A cm^{-2})	C.R., (mm/year)	I.E. (%)	R_p (ohm. cm^2)
Blank	−0.643	0.318	0.033	1.19×10^{-5}	0.405	–	1096
NC	−0.674	0.024	0.556	8.47×10^{-6}	0.142	65	2509
PA	−1.0905	0.1715	0.11555	2.06×10^{-6}	0.032	92	10,867
PU	−1.028	0.053809	0.13272	4.38×10^{-8}	0.001	98	379,490
Blank-stress	−0.983	0.319	0.061	8.96×10^{-5}	3.03	–	249
NC	−1.039	0.514	0.067	1.80×10^{-5}	0.65	78.5	1444
PA	−1.173	0.321	0.055	1.35×10^{-5}	0.46	84.8	1507
PU	−1.113	0.501	0.108	6.24×10^{-7}	0.02	99.3	61,609

on numerous considerations such as; coupling effect, current density distribution, electrode surface uniformity, surface electrode roughness, and the physical and/or chemical nature of conductor substances [32]. Plots of Bode Fig. 3b, c break up into three sections. The first one represents the solution resistance R_s at HF. The second part, in the medium frequency region, represents a capacitive behavior but not an ideal capacitor. In the last part at LF, the electrode resistance increases, and |Z| values do not depend on the frequency for uncoated and PU coating. The uncoated Al alloy is assigned to the Al_2O_3 layer resistance. The results display the untreated and treated Al alloy phase angle diagram as exhibited in Fig. 4a, b. The wide peak of high value 80° observed on the phase bode plot at PU coating is indicative of high corrosion protection at higher frequencies. For stress corrosion, the same tools were performed. Figure 4c shows the Nyquist plots for the untreated sample in NaCl. It is noticed that the impedance declines with increasing the stress from 100 to 175, and the diffusion appears in 175 stresses and dispersion suggests that, the start of metastable pitting [36–38].

Furthermore, due to microscopic surface irregularity and the existence of a spongy weathering creation film. Figure 5, the phase plot illustrates that the phase angle decreases from the blank sample to the 175-stress sample from 75 to 180. The plots of coated alloy as exhibited in Figs. 5, 6 represent that the Nyquist and bode plots the impedance increase in order NC, PA then PU. And Fig. 7 shows the phase value of PU-coated equal 60 and it is higher than other polymers but still lower than without stress. The organic coatings thus acted as efficient natural walls to avoid the attacked ions from infiltrating the coat into the electrolyte to cause alloy corrosion [39].

R_1 and R_2 in upper case: are the outer and inner layer resistance of Q_1 and Q_2 in μF cm^{-2}, respectively. ω is the angular frequency, J = About − 1: the imaginary component

$n1$ and $n2$ is the non-ideal constituent of the outer and inner layer capacities, respectively.

The diffusion process may be initiated by the diffusion of Al^{3+} cations from the metallic superficial to the wholesale environment under stress, which is created by the anodic reaction. EIS spectrum was fitted using a two-time measurements electrical equivalent circuit as displayed in Fig. 8a. R_s corresponds to the solution resistance; R_1 is the film resistance, C_1 is the capacitance of the coating film, R_2 is the R_p charge transfer, C_2 is the double-layer capacitance. The barrier properties of the coating can be evaluated through the pore resistance values R_1 obtained from modeling electrochemical impedance diagrams. The resistance of pores indicates the ease with which the electrolyte penetrates inside the coating see Table 3. The n component is compensate for the non-ideality of the roughness of the surface, the adsorption, and the incomplete homogeneity [40].

The equivalent circuit was used to fit the (a) corrosion behavior and (b) stress corrosion behavior of uncoated and coated Al7075 alloy immersed in 3.5% NaCl solution. R_s represents solution resistance used in the test, CPE is constant phase angle element, R_{ct} and W is charge transfer resistance, and Warburg impedance, respectively. The corresponding circuits Fig. 8a, b were used to match the untreated and treated Al7075 alloy's stress corrosion behavior plunged into a 3.5% NaCl solution. R_s characterize the solution resistance, CPE is the constant phase angle part, R_{ct} and W are the resistance to transfer charges, and Warburg impedance, respectively. In general, the constant phase element CPE uses instead of the pure double-layer capacitor to give a more accurate fit in the equivalent circuit. The correct value of double-layer capacitance C_{dl} was determined at the frequency f_{max}, at which the imaginary element of the impedance [41]. It is clear that, is the solution resistance R_s values increased in presence of polymer coating. it refers to a decrease in the conductivity of the solution. The R_{ct} values
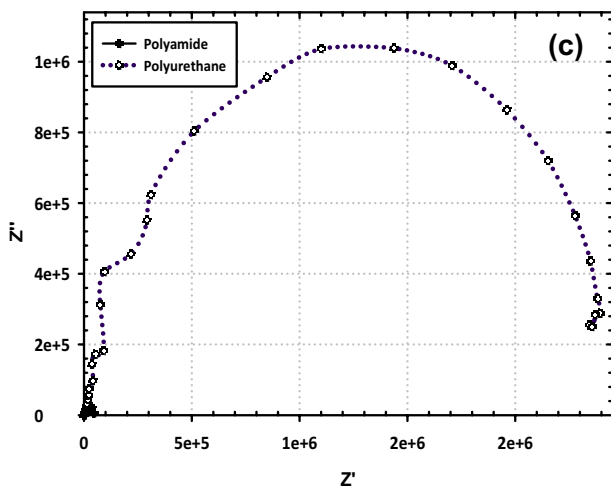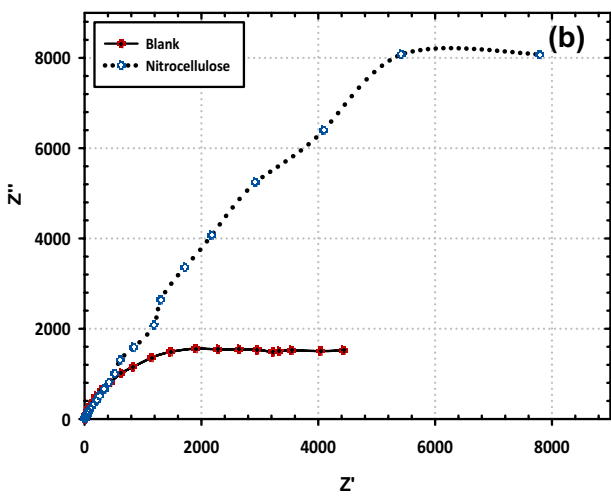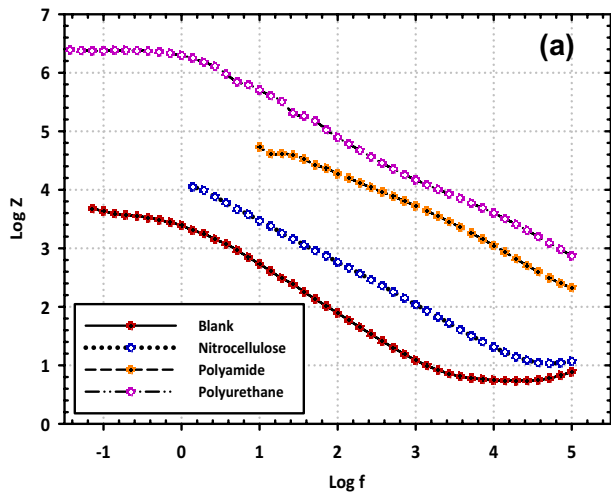
Fig. 3 Effect of coat on the **a** Bode plots of electrochemical impedance spectra of Al 7075 alloy in 3.5% NaCl solution. **b**, **c** Nyquist plots of electrochemical impedance spectra of Al 7075 alloy in 3.5% NaCl solution at ambient temperature
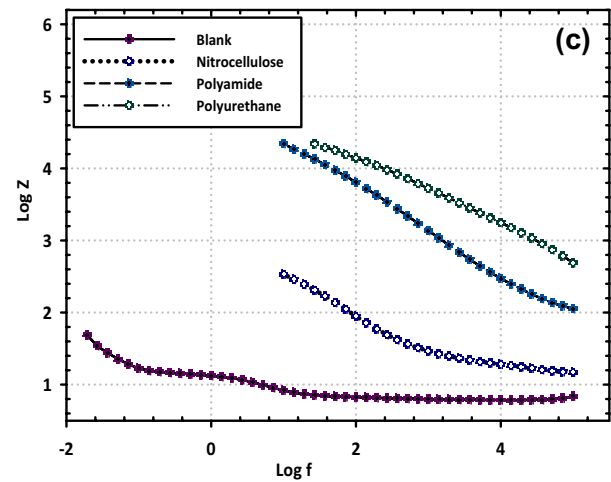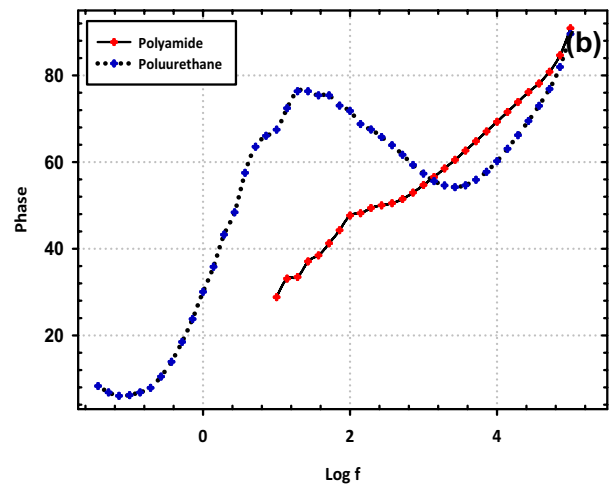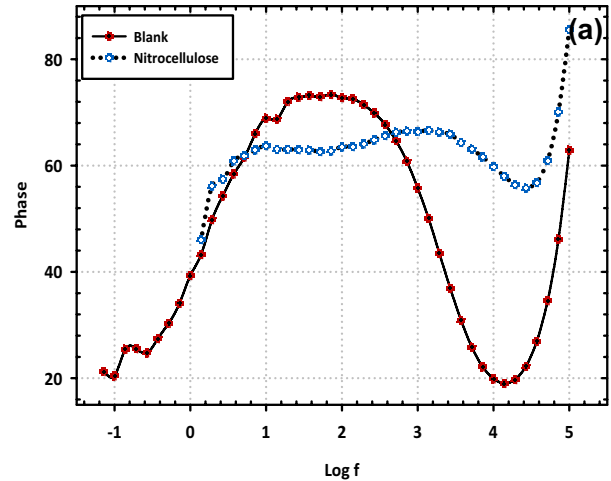
Fig. 4 Effect of coat on the **a**, **b** phase of electrochemical impedance spectra of Al 7075 alloy in 3.5% NaCl solution. **c** Bode plots of electrochemical impedance spectra of stress corrosion of Al 7075 alloy in 3.5% NaCl solution at ambient temperature
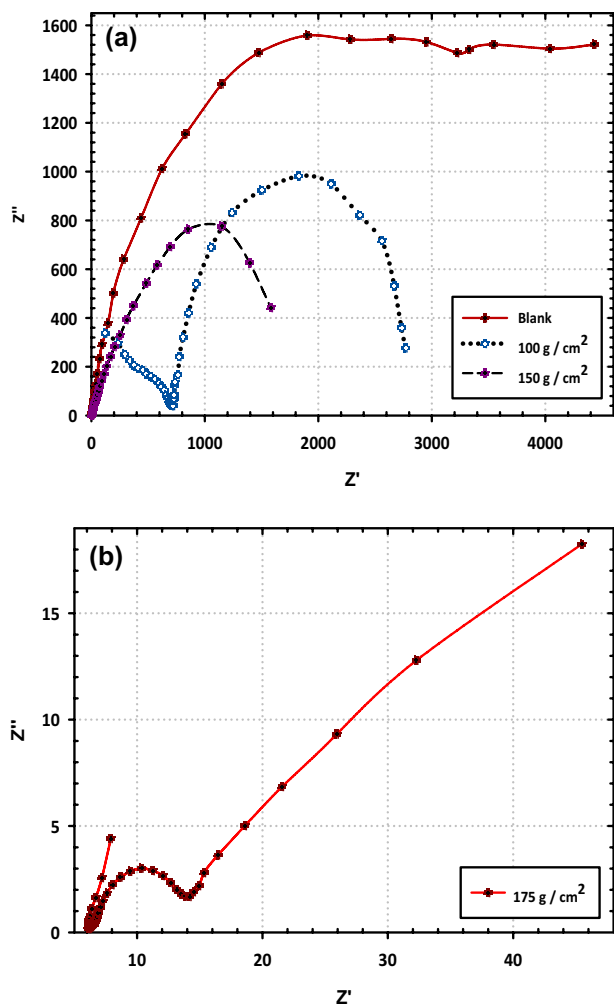
Fig. 5 Effect of coat on the Nyquist plots of electrochemical impedance spectra of stress corrosion of Al 7075 alloy in 3.5% NaCl solution at ambient temperature

increased indicating the formation of protective. Table 4 demonstrates the higher resistance value for the covering is up to 2.69×10^3 KΩ cm^2 with 99% efficiency.

It can be strong-minded that the treatment of uncoated samples in corrosive media, therefore, increases the capacity of the Al7075 alloys surface layer and, in the circumstance of PU, the thinness of the transfer of charge decreases by 99% concerning its performance. However, in the attendance of polymeric paint, the increased semicircular is regarded as an indicator of the R_p between the metal and the external Helmholtz plane. This event undistinguished the shielding layer on the superficial of the Al7075 alloy and therefore reduces the dissolution cycle. Both EIS results and Tafel results confirmed the order: PU>PA>NC> uncoated [42].

Fig. 6 Effect of coat performance on the **a**, **b** phase of electrochemical impedance spectra of stress corrosion of Al 7075 alloy in 3.5% NaCl solution. **c** Bode plots of stress corrosion of Al 7075 alloy in 3.5% NaCl solution at 175 g cm^{-2} at ambient temperature
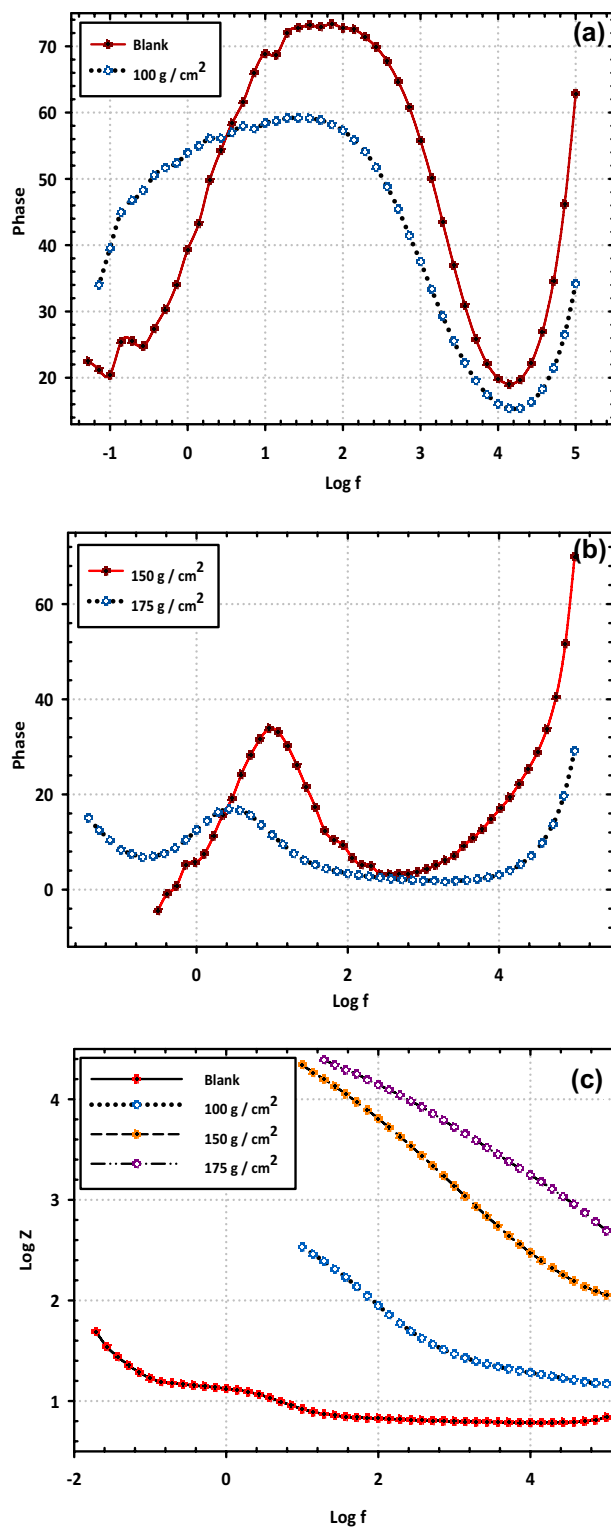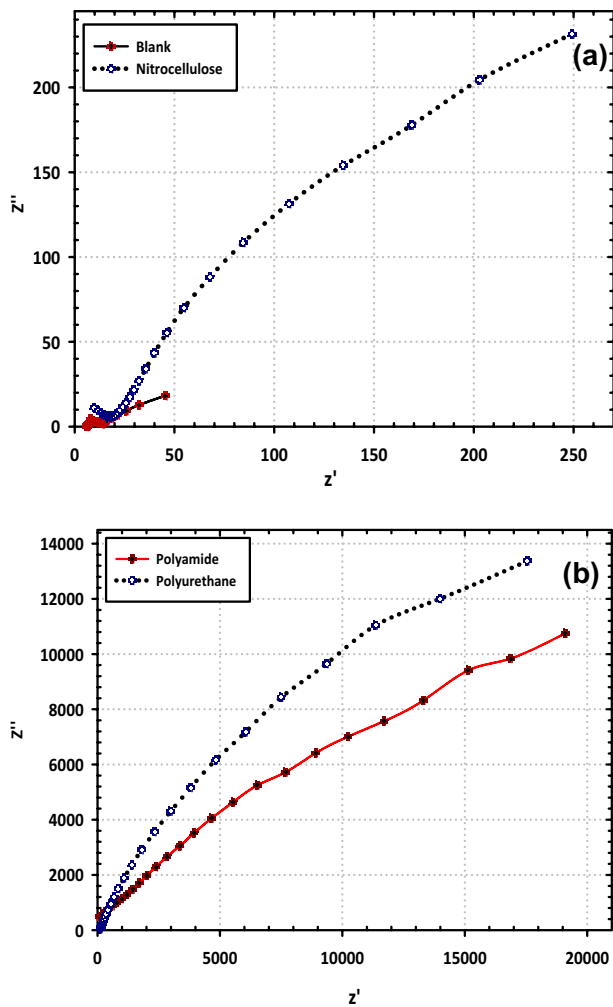
Fig. 7 Effect of coat performance on the Nyquist plots of electrochemical impedance spectra of stress corrosion of Al 7075 alloy in 3.5% NaCl solution at 175 g cm^{-2} at ambient temperature

3.4 Microstructure Characterization

Results exposed in Fig. 9a reveal that the polished sample of Al7075 electrode and the corroded sample in saline media is mentioned in Fig. 9b as well as the stress corroded sample at 175 g cm^{-2}. It is identified that, underwent energetic dissolution, as designated by the superficial coarseness in the untreated specimens with the polymer as mentioned in Fig. 9c. It is beyond that, with no insignia of pitting attack, and the formed rust has existed via general corrosion [37].
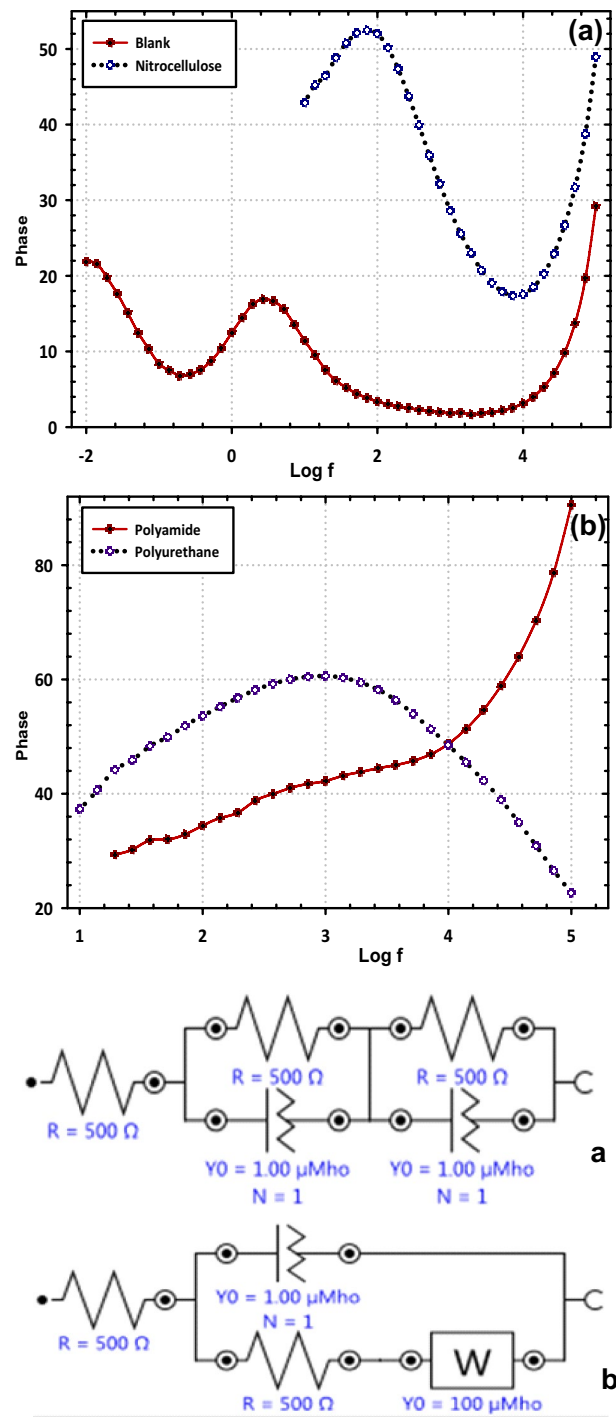

Fig. 8 Effect of coat performance on the phase of electrochemical impedance spectra of corrosion and stress corrosion of Al 7075 alloy in 3.5% NaCl solution at 175 g cm^{-2} at ambient temperature

Table 3 Electrochemical impedance parameters and inhibition efficiency of corrosion for coated and uncoated Al 7075 alloy in 3.5% NaCl

Materials	R_s	R_1	Q_1	n	R_2	Q_2	n	$E\%$
Blank	6.4	25	0.0036	0.74	5120	9.31×10^{-5}	0.80	–
NC	7.1	1.38	0.0001	0.56	16,470	1.23×10^{-5}	0.76	68
PA	10.1	706	9.94×10^{-5}	0.90	52,813	9.67×10^{-7}	0.63	90
PU	18.9	9.9×10^{7}	1.28×10^{-5}	0.85	2.69×10^{6}	9.92×10^{-8}	0.73	99
Blank-stress	6.4	25.0	0.0036	0.74	5120	9.31×10^{-5}	0.80	–
100 g cm^{-2}	19.8	683.6	1.72×10^{-7}	0.74	2885	7.84×10^{-5}	0.95	66.4
150 g cm^{-2}	6.31	105.77	0.791	0.4	2100	1.72×10^{-4}	0.76	57.2
175 g cm^{-2}	6.42	107.61	0.0078	0.67	7.44	1.51×10^{-3}	0.77	56.2

Table 4 Electrochemical impedance parameters and inhibition efficiency of stress corrosion at 175 for coated and uncoated Al7075 alloy in 3.5% NaCl

Materials at 175 g cm^{-2}	R_s	R_1	Q_1	n	R_2	Q_2	n	$E\%$
Blank	6.4	25	3.6×10^{-3}	0.74	5120	9.31×10^{-5}	0.80	–
Blank-stress	6.51	25.42	0.0252	0.67	7.44	10.3×10^{-5}	0.71	–
NC	9.8	10.34	1.54×10^{-6}	0.90	990.5	1.2×10^{-4}	0.72	48.3
PA	62.2	900	1.24×10^{-6}	0.6	99,900	3.5×10^{-6}	0.52	94.8
PU	42.3	5012	1.16×10^{-6}	0.7	1.25×10^{2}	3.2×10^{-6}	0.81	95.9

Furthermore, the roughness of the Al surface is seen to decrease in the polymer-coated sample, which represents prevention or guideline of the influence of corrosive media on the superficial of Al outstanding to the creation of protective deposits as seen in Fig. 9d for NC, Fig. 9e for PA and finally Fig. 9f for PU coat. The PU reveals the highest performance for corrosion resistance in saline solutions in both corrosion and stress corrosion [43].

4 Conclusions

This work describes the efficiency of sequences of coating materials of PU, PA, and NC in protection against corrosion. The R_p increased, while corrosion rate and corrosion current are diminished by PU coating, confirming that PU coating acts as an operative shield against deterioration of Al7075, suggesting the excessive possibility for application in industry. The investigational plots indicated that the crash tip-up tension rate and crack rapidity-based stress corrosion are restrained at the functional stress rate. In addition, the crack speed depended on the crack tip tension rate and the functional stress rate and was not predisposed in this study by the arrangement of the assessed Al sheet. It is also defined the consequences data of coated samples, that the rate of crack tip tension regulated the limiting rate of cracking from the stress corrosion of coated electrodes. The PU is recommended for application in coating the Al alloys to be protected in corrosive media since it is proved that gives a perfect resistant coat under stressed conditions.
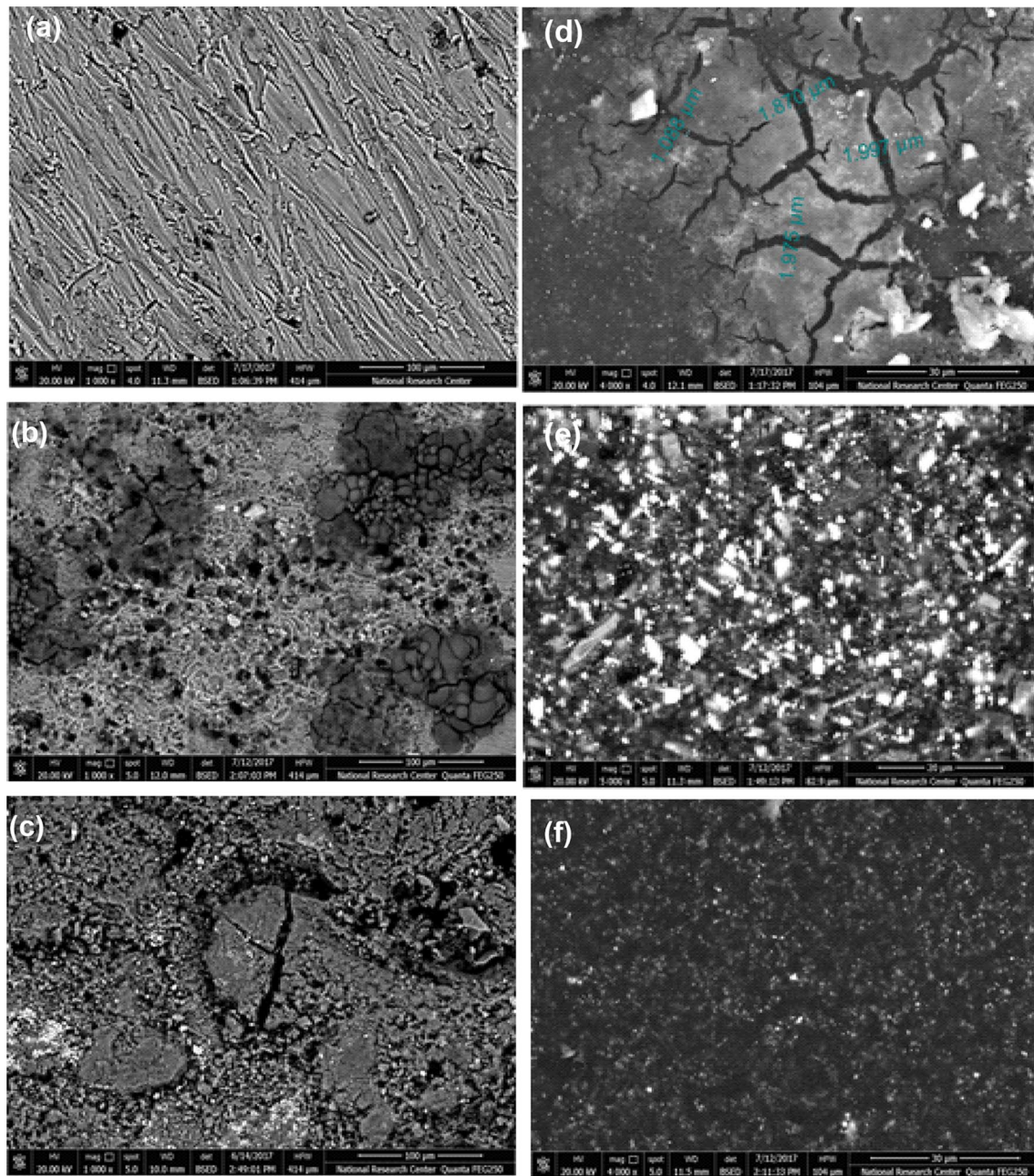
Fig. 9 SEM images of the Al7075 **a** polished sample, **b** uncoated sample, **c** uncoated sample under stress conditions, **d** NC-coated sample, **e** PA coated sample, and **f** PU-coated sample under stress conditions in 3.5% NaCl solution

Declarations

References

1. Tian W, Li S, Wang Bo, Liu J, Mei Yu (2016) Pitting corrosion of naturally aged AA 7075 aluminum alloys with bimodal grain size. Corros Sci 113:1–16
2. Mirhashemihaghighi S, Swiatowska J, Maurice V, Seyeux A, Zanna S, Salmi E, Ritala M, Marcus P (2016) Corrosion protection of aluminum by ultra-thin atomic layer deposited alumina coatings. Corros Sci 106:16–24
3. Reda Y, Zohdy KM, Eessaa AK, El-Shamy AM (2020) Effect of plating materials on the corrosion properties of steel alloy 4130. Egypt J Chem 63(2):579–597

4. Reda Y, El-Shamy AM, Zohdy KM, Eessaa AK (2020) Instrument of chloride ions on the pitting corrosion of electroplated steel alloy 4130. Ain Shams Eng J 11:191–199

5. Reda Y, El-Shamy AM, Eessaa AK (2018) Effect of hydrogen embrittlement on the microstructures of electroplated steel alloy 4130. Ain Shams Eng J 9(4):2973–2982

6. Eessaa AK, El-Shamy AM, Reda Y (2018) Fabrication of commercial nanoporous alumina by low voltage anodizing. Egypt J Chem 61(1):175–185

7. Knight SP, Birbilis N, Muddle BC, Trueman AR, Lynch SP (2010) Correlations between intergranular stress corrosion cracking grain-boundary microchemistry, and grain-boundary electrochemistry for Al–Zn–Mg–Cu alloys. Corros Sci 52:4073–4080

8. Sun XY, Zhang B, Lin HQ, Zhou Y, Sun L, Wang JQ, Han EH, Ke W (2013) Correlations between stress corrosion cracking susceptibility and grain boundary microstructures for an Al-Zn-Mg alloy. Corros Sci 77:103–112

9. Knight SP, Pohl K, Holroyd NJH, Birbilis N, Rometsch PA, Muddle BC, Goswami R, Lynch SP (2015) Some effects of alloy composition on stress corrosion cracking in Al-Zn-Mg-Cu alloys. Corros Sci 98:50–62

10. Su J, Zhang Z, Shi Y, Yang Z, Zhang J, Cao C (2006) The effect of applied tensile stress on the exfoliation corrosion of 7075–T6 alloy. Mater Corros 57:729–733

11. Adler PN, Delasi R, Geschwind G (1972) Influence of microstructure on mechanical properties and stress-corrosion susceptibility of 7075 aluminum alloy. Metall Trans 3:3191–3200

12. Puiggali M, Zielinski A, Olive JM, Renauld E, Desjardins D, Cid M (1998) Effect of microstructure on stress corrosion cracking of an Al–Zn–Mg–Cu alloy. Corros Sci 40:805–819

13. Sabelkin V, Perel VY, Misak HE, Hunt EM, Mall S (2015) Investigation into crack initiation from corrosion pit in 7075–T6 under ambient laboratory and saltwater environments. Eng Fract Mech 134:111–123

14. El-Shamy AM, Abdelfattah I, Elshafey OI, Shehata MF (2018) Potential removal of organic loads from petroleum wastewater and its effect on the corrosion behavior of municipal networks. J Environ Manag 219:325–331

15. El-Shamy AM, El-Boraey HA, El-Awdan HF (2017) Chemical treatment of petroleum wastewater and its effect on the corrosion behavior of steel pipelines in sewage networks. J Chem Eng Process Technol 8:1

16. Johansen HD, Brett CMA, Motheo AJ (2012) Corrosion protection of aluminum alloy by cerium conversion and conducting polymer duplex coatings. Corros Sci 63:342–350

17. El-Shamy AM, Zohdy KM, El-Dahan HA (2016) Control of corrosion and microbial corrosion of steel pipelines in salty environment by polyacrylamide. Ind Chem 2:2

18. Altin A, Rohwerder M, Erbe A (2017) Cyclodextrins as carriers for organic corrosion inhibitors in organic coatings. J Electrochem Soc 164(4):C128–C134

19. Santos D, Brites C, Coasta MR, Santos MT (2005) Performance of paint system with polyurethane (PU) topcoats, proposed for atmospheres with very high corrosivity category. Prog Org Coat 54(4):344–352

20. Shanab SMM, Ameer MA, Fekry AM, Ghoneim AA, Shalaby EA (2011) Corrosion resistance of magnesium alloy (AZ31E) as orthopedic biomaterials in sodium chloride containing antioxidantly active compounds from eichhorniacrassipes. Int J Electrochem Sci 6:3017–3035

21. Zhang W, Gao L, Lia J, Yang J, Yin Y (2011) TiAl/B4C marine material-fabrication, mechanical and corrosion properties'. Ceram Int 37:783–789

22. Ma H, Cheng X, Li G, Chen S, Quan Z, Zhao S, Niu L (2000) The influence of hydrogen sulfide on corrosion of iron under different conditions. Corros Sci 42:1669–1683

23. Zohdy KM, El-Sherif RM, Ramkumar S, El-Shamy AM (2021) Quantum and electrochemical studies of the hydrogen evolution findings in corrosion reactions of mild steel in acidic medium. Upstream Oil Gas Technol 6:100025. https://doi.org/10.1016/j.upstre.2020.100025

24. El-Shamy AM, El-Hadek MA, Nassef AE, El-Bindary RA (2020) Optimization of the influencing variables on the corrosion property of steel alloy 4130 in 3.5 wt.% NaCl solution. J Chem. https://doi.org/10.1155/2020/9212491

25. Danaee I, Niknejad Khomami M, Attar AA (2013) Corrosion of AISI 4130 steel alloy under hydrodynamic condition in ethylene glycol + water + NO_2^{-2} solution. J Mater Sci Technol 29:89–96

26. Ettefagh Far SH, Davoodi A (2014) Microstructure and corrosion behavior of plain carbon steel–B4C composite produced by GTAW method in 3.5 wt-%NaCl solutions. Corros Eng Sci Technol 49(1):55–65

27. Baragetti S, Gerosa R, Villa F (2016) Step loading corrosion fatigue testing of 7075–T6 WC/C coated specimens in air and methanol. Eng Fract Mech 164:106–116

28. Marin de Camargo JA, Voorwald HJC, Hilário Cioffi MO, Pitanga Costa MY (2007) Coating residual stress effects on fatigue performance of 7050–T7451 aluminum alloy. Surf Coat Technol 201:9448–9455

29. Huang Y, Ye X, Benrun Hu, Chen L (2016) Equivalent crack size model for pre-corrosion fatigue life prediction of aluminum alloy 7075–T6. Int J Fatigue 88:217–226

30. Gao H, Zhang Y, Qiong Wu, Song J, Wen K (2018) Fatigue life of 7075–T651 aluminium alloy treated with vibratory stress relief. Int J Fatigue 108:62–67

31. Wang H, Ning C, Huang Y, Cao Z, Chen X, Zhang W (2017) Improvement of abrasion resistance in artificial seawater and corrosion resistance in NaCl solution of 7075 aluminum alloy processed by laser shock peening. Opt Lasers Eng 90:179–185

32. Xie L, Jiang C, Lu W, Zhan K, Chen Y (2011) Investigation on the residual stress and microstructure of (TiB+TiC)/Ti–6Al–4V composite after shot peening. Mater Sci Eng A 528:3423–3427

33. Gomez-Rosas G, Rubio-Gonzalez C, Ocaña JL, Molpeceres C, Porro JA, Chi-Moreno W (2005) High level compressive residual stresses produced in aluminum alloys by laser shock processing. Appl Surf Sci 252:883–887

34. Salimianrizi A, Foroozmehr E, Badrossamay M, Farrokhpour H (2015) Effect of laser shock peening on surface properties and residual stress of Al6061-T6. Opt Lasers Eng 77:112–117

35. Meydanoglu O, Bertrand Jodoin E, Kayali S (2013) Microstructure, mechanical properties and corrosion performance of 7075 Al matrix ceramic particle reinforced composite coatings produced by the cold gas dynamic spraying process. Surf Coat Technol 235:108–116

36. Li Y, Zhang P, Bai P, Liyun Wu, Liu B, Zhao Z (2018) Microstructure and properties of Ti/TiBCN coating on 7075 aluminum alloy by laser cladding. Surf Coat Technol 334:142–149

37. Meng X, Lin Z, Wang F (2013) Investigation on corrosion fatigue crack growth rate in 7075 aluminum alloy. Mater Des 51:683–687

38. Vaibhav Pandey JK, Singh K, Chattopadhyay NCS, Srinivas VS (2017) Influence of ultrasonic shot peening on corrosion behavior of 7075 aluminum alloy. J Alloy Compd 723:826–840

39. Harrison TJ, Crawford BR, Brandt M, Clark G (2014) Modelling the effects of intergranular corrosion around a fastener hole in 7075–T651 aluminum alloy. Comput Mater Sci 84:74–82

40. El-Shamy AM, Shehata MF, Gaballah ST, Elhefny EA (2014) Synthesis and evaluation of ethyl (4-(n-(thiazol-2-yl) sulfamoyl) phenyl) carbamate as a corrosion inhibitor for mild steel in 0.1M HCl. J Adv Chem 11(2):3441–3451

41. Zohdy KM, El-Sherif RM, El-Shamy AM (2021) Corrosion and passivation behaviors of tin in aqueous solutions of

different pH. J Bio- Tribo-Corros 7(2):1–7. https://doi.org/10.1007/s40735-021-00515-6

42. Abdel-Karim AM, El-Shamy AM (2022) A review on green corrosion inhibitors for protection of archeological metal artifacts. J Bio- Tribo-Corros 8:35. https://doi.org/10.1007/s40735-022-00636-6

43. Reda Y, Yehia HM, El-Shamy AM (2022) Microstructural and mechanical properties of Al-Zn alloy 7075 during RRA and triple aging. Egypt J Pet 31:9–13. https://doi.org/10.1016/j.ejpe.2021.12.001